

THE ASTEROID DISTRIBUTION IN THE ECLIPTIC

ERIN LEE RYAN¹, CHARLES E. WOODWARD¹, ANDREA DIPAOLO², JACOPO FARINATO³, EMANUELE GIALLONGO², ROLAND GREDEL⁴, JOHN HILL⁵, FERNANDO PEDICHINI², RICHARD POGGE⁶, ROBERTO RAGAZZONI³

ABSTRACT

We present analysis of the asteroid surface density distribution of main belt asteroids (mean perihelion $\Delta \simeq 2.404$ AU) in five ecliptic latitude fields, $-17 \gtrsim \beta(^{\circ}) \lesssim +15$, derived from deep *Large Binocular Telescope* (LBT) *V*-band (85% completeness limit $V = 21.3$ mag) and *Spitzer Space Telescope* IRAC 8.0 μm (80% completeness limit $\sim 103 \mu\text{Jy}$) fields enabling us to probe the 0.5–1.0 km diameter asteroid population. We discovered 58 new asteroids in the optical survey as well as 41 new bodies in the *Spitzer* fields. The derived power law slopes of the number of asteroids per square degree are similar within each $\sim 5^{\circ}$ ecliptic latitude bin with a mean value of -0.111 ± 0.077 . For the 23 known asteroids detected in all four IRAC channels mean albedos range from 0.24 ± 0.07 to 0.10 ± 0.05 . No low albedo asteroids ($p_V \lesssim 0.1$) were detected in the *Spitzer* FLS fields, whereas in the SWIRE fields they are frequent. The SWIRE data clearly samples asteroids in the middle and outer belts providing the first estimates of these km-sized asteroids' albedos. Our observed asteroid number densities at optical wavelengths are generally consistent with those derived from the Standard Asteroid Model within the ecliptic plane. However, we find an over density at $\beta \gtrsim 5^{\circ}$ in our optical fields, while the infrared number densities are under dense by factors of 2 to 3 at all ecliptic latitudes.

¹Department of Astronomy, School of Physics and Astronomy, 116 Church Street, S. E., University of Minnesota, Minneapolis, MN 55455, ryan@astro.umn.edu, chelsea@astro.umn.edu

²Osservatorio Astronomico di Roma, via di Frascati 33, I-00040 Monteporzio, Italy

³Osservatorio Astronomico di Padova, vicolo dell'Osservatorio 5, I-35122 Padova, Italy

⁴Max-Planck-Institut fuer Astronomie, Koenigstuhl 17, D-69117 Heidelberg, Germany

⁵Large Binocular Telescope Observatory, University of Arizona, 933 N Cherry Ave, Tucson, AZ, 85721-0065

⁶Department of Astronomy, The Ohio State University, 140 W. 18th Avenue, Columbus, OH 43210-1173

Subject headings: Infrared: solar system – minor planets, asteroids – surveys

1. INTRODUCTION

The present main belt asteroid size distribution provides important constraints on models of the original size distribution of planetesimals and their collisional evolution. The size-frequency distribution, main belt asteroid scale height, and albedo variations extant in a large, well-sampled population are also essential to model the size distribution of the Near Earth Asteroid (NEA) population and to determine the evolution of main belt objects as compared to those bodies injected into Earth crossing orbits (e.g., Trilling et al. 2008).

Most main belt asteroids are found between 2.2 and 3.4 AU from the sun and at ecliptic latitudes nominally less than 20° . The size-frequency distribution of main belt asteroids with diameters < 1 km is essentially unknown due to observational flux limits. For asteroids with diameters > 1 km, the derived size-frequency distribution estimates range from 7×10^5 km-sized objects (optical Sloan Digital Sky Survey, SDSS; Abazajian et al. 2004; Ivezić et al. 2001) to $(1.2 \pm 0.5) \times 10^6$ km-sized objects (derived from surveys with the *Infrared Space Observatory*, ISO; Tedesco & Desert 2002) within the main belt. Recently, Stapelfeldt et al. (2006) have derived a size-frequency estimate for the > 1 km-sized bodies for two fields at 0° and 10° ecliptic latitude from $24 \mu\text{m}$ photometry obtained with the NASA *Spitzer Space Telescope* (*Spitzer*, Gehrz et al. 2007; Werner et al. 2004) that concurs with values derived from analysis of the Sloan fields. While the infrared (IR) and optical methodologies yield comparable size estimates, these surveys are potentially biased as they are unable to detect (either through intrinsic sensitivity limits or survey design) fainter objects within the main belt. Thus, the size-frequency distribution may not be complete due to the preferential selection of a cross section of the asteroid population with high albedo values or large sizes.

Bottke et al. (2005) have modeled the collisional evolution of the size distribution of the main belt using the current size-frequency distributions within the main belt as well as the size-frequency distribution of NEAs to constrain the primordial asteroid distribution. Their best-fit models, based on the current size-frequency distribution, predict $\simeq 10^6$ asteroids within the 0.3 to 1 km size range. Collisional models by O’Brien & Greenberg (2005) predict $\simeq 10^5$ bodies in a similar size range within the main belt. However, the validity of the population extrapolation is based on an accurate understanding of the current size-frequency distribution necessitating deep observations to provide accurate number counts at both optical wavelengths (higher albedo objects) and IR (larger dark asteroids) wavelengths. The collisional evolution model by Bottke et al. (2005) suggests that the primordial main belt contained ~ 150 to 250 times the current population of objects with diameters, $D \lesssim 1000$ km.

The Bottke et al. (2005) model produces a parent population of similar magnitude to that required by interpretation of the meteoritic record. For instance Wetherill (1989) argues that the surface density within the main belt must be at least 100 times higher than that currently observed to be consistent with the meteoritic record. The total mass of known asteroids in the main belt is $5 \times 10^{-4} M_{\oplus}$. However, both the meteoritic record and collisional models require a primordial main belt mass of $7.5 \times 10^{-2} M_{\oplus}$ to $1.25 \times 10^{-1} M_{\oplus}$. The significant discrepancy between the mass of the primordial main belt and the current mass, primarily derived from large ($D \geq 10$ km) sized asteroids, may be resolved by extending the asteroid number census to properly encompass smaller sizes while including populations found at higher ecliptic latitudes.

Here we present new observational results to constrain the size-frequency distribution of main belt asteroids and their ecliptic scale-height derived from a deep optical survey of select ecliptic fields obtained with the *Large Binocular Telescope* (LBT) as well as near- and mid-IR fields observed with *Spitzer* drawn from the data archive. Section 2 describes our observations and reduction techniques, §3 discusses the newly discovered asteroids and our derivation albedo, size-frequency distribution, and scale-height, while §4 summarizes our conclusions.

2. OBSERVATIONS & ARCHIVAL ANALYSIS

2.1. LBT Observations

Optical observations were obtained at the Large Binocular Telescope (LBT; Hill et al. 2006) facility of the Mt. Graham International Observatory with the blue channel of the Large Binocular Camera (LBC; Ragazzoni et al. 2006; Giallongo et al. 2008) and a single 8.4 m mirror on various nights during 2007 January 16 through 24 UT as part of Science Demonstration Time (SDT) activities. The LBC is a wide-field imager incorporating four 2048×4608 pixel CCD detectors with a $23' \times 23'$ field of view (FOV) and a $0.23''$ per pixel platescale. Four fields at ecliptic latitudes of 0° , 5° , 10° , and 15° were observed using a series of 4 min exposures in the V-band ($\lambda_o = 0.55 \mu\text{m}$; $\Delta\lambda = 0.094 \mu\text{m}$) under non photometric conditions with seeing between $\simeq 1.3'' - 3.0''$. Fields were selected to be at solar elongations near 160° , such that sufficient asteroid motion on the plane of the sky could be detected within the ~ 3 hr observational baseline. Observations of each field consisted of 2 pointings, with one pointing offset by $\sim 7.85'$, resulting in a total areal coverage per field of 0.2835 square degrees. Table 1 provides complete observational details.

The data were reduced using standard IRAF¹ routines in the *mscred* package. Images were trimmed, bias-subtracted, and flat-fielded using median sky flats created with twilight flats and additional data obtained during 2007 January SDT time. Astrometric solutions for each data frame were generated using IRAF routines, in conjunction with the stellar positions obtained from the USNO A2.0 astrometric catalog (Zacharias et al. 2004). The solutions had a positional accuracy of $0.25'' \pm 0.08''$ for each field and the relative position of detected asteroids are referenced to this grid.

Asteroid detection was performed using a three color method. Images with astrometric solutions were displayed in image display tool DS9 (Joye & Mandel 2003), with each individual epoch (Table 1) loaded into a different color table. Asteroids were identified by pairs or triplets of individually colored sources. From these identifications, absolute pixel coordinates for each target were obtained, which were subsequently used for photometric measurements. Due to the conditions under which the data was obtained, a high signal to noise of 10 is required for any asteroid detection. Secondary confirmation of this asteroid detection technique was performed by registering individual epoch frames by the world coordinate system (WCS) and then subtracting, leaving positive and negative asteroid pairs. While this latter technique would be preferred over the three color technique, the seeing varied by $1.3''$ to $3.0''$ over each night causing the WCS subtraction technique to be less reliable.

Photometry was performed using a circular aperture with a radius of 10 pixels for each asteroid coordinate. The photometry was calibrated from stellar sources in the fields using published V -band magnitudes taken from the Tycho and USNO A2.0/YB6 catalogs (mean photometric errors of the order $\lesssim 0.1$ mag). Forty stars (10 stars per chip) were identified by their astrometric positions and were used to find a photometric offset between the measured and reported absolute values from Tycho/USNO A2.0. This zero-point photometric offset, which includes the mean photometric error, was then used to calibrate the asteroid photometry in each pointing as described in Table 1, column [7].

We detected 62 asteroids in the LBC V -band images, of which only four are previously known objects with orbital determinations. The 58 newly discovered asteroids detected in this survey were observed in either two or three epochs. Due to the field overlap between pointings, some asteroids were detected six times, allowing for both precise astrometry and photometry. Table 2 summarizes the number of asteroids found in each field as well as the extrapolated number counts per square degree at each latitude and the limiting magnitudes

¹IRAF is distributed by the National Optical Astronomy Observatories, which are operated by the Association of Universities for Research in Astronomy, Inc., under cooperative agreement with the National Science Foundation.

for each field. The extrapolated optical number counts were obtained by multiplying the asteroid number counts in a field by the number 0.2835 square degree fields necessary to tile a 1 square degree field assuming a uniform asteroid density at each latitude.

2.2. *Spitzer* Archival Fields

Asteroid photometry and number counts in select ecliptic fields discussed in §3 were derived from new ground-based optical observations and point-sources extractions obtained from fields observed with the Infrared Camera (IRAC; Fazio et al. 2004) and the Multiband Infrared Photometer for *Spitzer* (MIPS; Rieke et al. 2004) as part of various IR survey programs retrieved in the *Spitzer* public archive.

Post-pipeline (pipeline v15) basic calibrated data (BCDs) of selected *Spitzer* IRAC fields were downloaded from the public archive and utilized for asteroid detection. Fields were selected from the ecliptic plane component of the *Spitzer* First Look Survey (FLS, program identification (PID) 98; Meadows et al. 2004), and SWIRE XMM-LSS fields (PID 181; Lonsdale et al. 2003). IRAC 8.0 μm data is preferable for asteroid detection due to the detector platescale ($\simeq 1.2''$) and detector sensitivity. The 5σ detection limit for a 500 sec IRAC 8.0 μm observation is 27 μJy , enabling detection of small main belt asteroids with high signal-to-noise ratios (SNR) in short integration times. For example, the 8.0 μm flux from a 1 km diameter main belt asteroid radiating as a blackbody with an orbital semi-major axis of 2.5 AU (3.2 AU) viewed at opposition is $\approx 1096 \mu\text{Jy}$ ($\approx 20.1 \mu\text{Jy}$). Once an asteroid candidate is identified at 8.0 μm its sky coordinate can then be used to examine pixels at the same location in the IRAC 3.6, 4.5, and 5.8 μm images. Although the flux densities for small-sized asteroids near the outer belt edge are not easily detectable with IRAC in single frames at shorter wavelengths, their motion will separate them from the confusion caused by faint extragalactic sources or point spread function (PSF) smearing of the telescope.

Due to limits on observation durations (driven by on-board data storage issues and downlink frequency), the *Spitzer* deep large area surveys must consist of multiple epochs of data with multiple pointings. For asteroid detections this is advantageous as the observation duration limit for all IRAC observations is 6 hrs which allows observations to be repeated with a cadence of a few hours. Assuming circular Keplerian orbits within the asteroid belt, the angular velocity ω (rad s^{-1}), or rate of motion on the sky of an object near opposition is

$$\omega = \sqrt{\frac{GM_{\odot}}{R^3}} \quad (1)$$

where $G = 6.67 \times 10^{-11} \text{ m}^3 \text{ kg}^{-1} \text{ s}^{-2}$, M_{\odot} is the mass of the sun, and R is the orbital distance in meters. For inner main belt asteroids with a semi-major axis of 2.2 AU, the expected rate of motion is $45''$ per hr, while the expected rate of motion for outer main belt asteroids is $24''$ per hr. However, the actual rates and direction of motion on the sky may significantly differ from these values (e.g., near quadrature, when the FLS fields were observed at solar elongation $\simeq 115^\circ$). Nevertheless, movement on the sky of many tens of arcsec per hr enables one to detect asteroids in the field on timescales of hours.

The FLS consisted of IRAC observations of two 0.13 square degree fields ($10' \times 48'$) centered on a solar elongation of 115° as seen from *Spitzer*, at ecliptic latitudes $\beta = 0^\circ$ and $+5^\circ$ on 2004 January 21 UT. In J2000 coordinates, this corresponds to field centers of R.A. = $12^{\text{h}}03^{\text{m}}22.03^{\text{s}}$, decl. = $-00^\circ21'53.8''$ for the $\beta = 0^\circ$ field, and RA = $12^{\text{h}}11^{\text{m}}20.10^{\text{s}}$, decl. = $+04^\circ13'18.7''$ for the $\beta = +5^\circ$ field as viewed by *Spitzer*. To detect asteroid motion, each IRAC field was observed at three epochs separated by 70 min.

For each of the latitude fields, we colored each epoch and coadded the IRAC $8.0 \mu\text{m}$ mosaics of the three epochs using a fixed stellar WCS to create a composite red, green, blue (RGB) image, which was then examined. In this RGB image, fixed sources appear white, and moving targets were seen as red-green-blue quasi-linear sequences of sources. The typical SNR for the detected sources was $\gtrsim 10$. Using the RGB technique with the IRAC $8.0 \mu\text{m}$ data, we were able to identify 18 sources in the $\beta = 0^\circ$ field, and 16 sources in the $\beta = +5^\circ$ field. The faintest of these sources have $8.0 \mu\text{m}$ fluxes of $\simeq 80 \mu\text{Jy}$ and were detected with a SNR ~ 10 in both fields. For comparison, Meadows et al. (2004) identified 15 known (six of which we also recover) and 19 unknown asteroids their analysis of the FLS fields, reporting $8.0 \mu\text{m}$ fluxes ranging from 5.6 to 0.09 mJy.

The SWIRE program was designed to explore large scale structure in the universe with the IRAC and MIPS cameras (Lonsdale et al. 2004). This survey consisted of 6 fields selected to overlap those observed at depth in by the *Hubble Space Telescope* and the *Chandra X-Ray Observatory*. Two epochs of observations were obtained for each of the six fields to pre-empt moving targets from final mosaics enabling high fidelity point source catalogs to be generated. For the purposes of our asteroid survey we used IRAC data obtained between 2004 July 23 and 2004 July 28 in the SWIRE XMM-LSS field, located at $\beta = -17^\circ$ and encompassing an area of 9.1 square degrees. Due to the large area covered by this *Spitzer* survey and duration limitations of single observations, the IRAC data consists of 16 individual pointings of 0.44 square degrees in two epochs. The two epochs of each pointing are offset by 3.75 hrs, thus significant asteroid motion can be detected.

Asteroid detection in the SWIRE data sets was also performed by coloring and coadding IRAC $8.0 \mu\text{m}$ mosaics of each epoch to create a composite red-blue (RB) image. In this RB

image, fixed sources appear purple, and moving targets were seen as red-blue quasi-linear sequences of sources. We identify a total of 46 sources in the field. The faintest sources have $8.0 \mu\text{m}$ fluxes of $\simeq 300 \mu\text{Jy}$ and were detected with a $\text{SNR} \sim 20$ in both fields. Of the 46 sources detected, only 14 asteroids have ground based detections and orbital elements.

Fluxes in all four IRAC channels were obtained for all asteroids in the FLS and SWIRE datasets. Pixel coordinates for each asteroid were recorded at the time of detection and were used for photometry. Though the IRAC cameras have an offset between the $3.6/5.8 \mu\text{m}$ and the $4.5/8.0 \mu\text{m}$ FOVs, pipeline processed mosaics in each channel are aligned such that a given sky coordinate corresponds to the same pixel coordinate in all four channels. This allows use of one set of pixel coordinates for all sources in all 4 channels. Source photometry was performed using the IRAF task *phot* and a three-pixel radius circular aperture to measure the asteroid flux and a concentric four-pixel wide sky annulus to determine the median sky contribution to the total flux measured in the integrated object aperture. Final fluxes and flux uncertainties were derived using the aperture corrections contained in the IRAC Data Handbook (Spitzer Science Center 2006). Due to the offset in the IRAC channel FOVs, some asteroids are only detected in the 4.6 and $8.0 \mu\text{m}$ data. The number of asteroids detected in all four IRAC bands is 40 in the SWIRE data and 24 in the FLS fields. The mean (median) $8.0 \mu\text{m}$ asteroid fluxes are $315 \pm 78 \mu\text{Jy}$ ($199 \pm 78 \mu\text{Jy}$), $1276 \pm 680 \mu\text{Jy}$ ($302 \pm 608 \mu\text{Jy}$), and $2448 \pm 53 \mu\text{Jy}$ ($1355 \pm 53 \mu\text{Jy}$) for *Spitzer* FLS 0° , FLS 5° , and SWIRE fields respectively. The total number of asteroids detected in the *Spitzer* fields are summarized in Table 2.

Detailed physical parameters for the newly discovered asteroids detected at optical (58) and IR (41) wavelengths are presented in on-line machine-readable catalogs. Illustrative catalog layouts are shown in Table 3 and Table 4. The optical catalog, Table 3, is similar to the standard Minor Planet Center submission format². In our Table 3 the corresponding column format is used: [1] the asteroid name, [2] a true/false=1/0 flag indicating if asteroid is a new discovery, [3]–[5] are respectively the year, month and UT date of observation, [6]–[11] are the right ascension and declination (J2000.0) of the detected target, [12] and [13] are the observed asteroid magnitude and associated uncertainty, while [14] is the filter used for the observations. The IR machine-readable catalog, Table 4, is similar in column format where: [1] is the asteroid name, [2] is the *Spitzer* Program ID number, [3] is the astronomical observation request (AOR) key, [4]–[9] is the year, UT date and time at the start of an observation, [5] and [6] are the right ascension and declination in degrees, [10]–[13] are the right ascension and declination and ecliptic latitude and longitude in sexagesimal degrees, while [14] through [21] are the observed fluxes and flux errors in μJy measured

²<http://www.cfa.harvard.edu/iau/info/OpticalObs.html>

for each asteroid in the four IRAC channels. Note that the fluxes in the table are not color-corrected.

3. DISCUSSION

The distribution of asteroids within the main belt provides a means to ascertain the mass distribution of material within the main belt and provides constraints for theoretical models developed to describe planet formation from protoplanetary disks encompassing our own proto-sun, as well as those extant around other young stellar systems. By probing the asteroid distribution in reflected optical light and in the thermal IR in coordinated observational programs, a more complete picture of the number of asteroids and sizes and albedos can be obtained. Current models of solar system dynamics (e.g., Bottke et al. 2005) use the distribution of absolute magnitudes of asteroids combined with a single geometric albedo to estimate the size-frequency distribution of asteroids as observationally determined diameters and albedos of main belt asteroids only exist for ~ 2400 objects. However, new survey data now available from fields observed with the *Spitzer* can be used to determine asteroid albedos and diameters for sizes under 1 km, enabling a more robust determination of albedo trends and size as a function of latitude for a more representative population of objects (e.g., a broader sampling of the total distribution). Our study describes the first results for main belt asteroids with diameters of 0.5 km.

3.1. Completeness Limits

To test completeness of our optical and *Spitzer* data sets, we used the IRAF task *mkobjects* to create synthetic point sources in data frames. To assess completeness in the optical data, synthetic point sources were added with the same seeing values measured in each frame and with coordinates that varied to mimic asteroid motion. To model the *Spitzer* images, synthetic objects were randomly placed into an image with motions equivalent to the median rates of a body in Keplerian orbit at the corresponding ecliptic latitude. Synthetic asteroids were then recovered using the same RGB technique originally used to detected asteroids in the observational images. Our completeness values are not only sensitive to source fluxes, but also to motion. For valid completeness detection, an asteroid must be detected in at least 2 of the 3 epochs of data.

In our optical data, the 85% moving target completeness limit in all fields is $V = 21.3$. Because the moving target completeness samples the completeness due to (1) a limiting

flux and (2) motion, a point source completeness test was also performed. This exercise shows that the point source completeness at $V = 21.3$ is 90%. For all asteroids counts at magnitudes greater than 21.3, the difference in the two completeness values of 5%, is applied by assuming that the number of asteroids not detected due to motion is the same at all magnitudes. These completeness values have been used to obtain corrected asteroid number counts which are reported in column [3] in Table 2. Figure 1 shows the number counts per square degree as a function of magnitude in each optical field.

The *Spitzer* IRAC 8.0 μm analysis, under the constraints that the synthetic asteroid rate of motion was comparable to the median rates of motion in a field at a given ecliptic latitude combined with the requirement of a minimum of 2 detections per synthetic asteroid yields an 80% completeness limit for the FLS and SWIRE data for $F_{8\mu\text{m}} = 103 \mu\text{Jy}$. Our derived completeness value differs somewhat from that reported for the FLS by Meadows et al. (2004) who cite 90% completeness at 100 μJy based on fixed target detections. With the completeness limit at 103 μJy , we calculate that the number of asteroids in the FLS 0° and 5° fields are 148 ± 12 and 133 ± 12 per square degree respectively, and 5 ± 2 per square degree for the -17° SWIRE field. Figure 2 are histogram plots of the surface density of asteroids as a function of 8.0 μm flux in the *Spitzer* FLS and SWIRE fields.

3.2. Bulk size-frequency distribution

Comparison of these two major data sets in different wavelengths is complicated in part by the potential for a disparate probe of asteroid sizes. Using the completeness limits in the V -band and at IRAC 8.0 μm we can estimate the minimum radii of asteroids detectable in our survey from

$$F_{reflected} = \frac{2h\nu^3}{c^2} \frac{1}{e^{\frac{h\nu}{kT_\odot}} - 1} \frac{R_\odot}{r} \frac{Rp_v \pi D^2 \cos(\tilde{\alpha})}{16\pi\Delta^2} \quad (2)$$

and

$$F_{thermal} = \frac{2\epsilon D^2 h\nu^3}{d_{Spitzer}^2 c^2} \left[\int_0^{\frac{\pi}{2}} \int_{-\frac{\pi}{2}}^{\frac{\pi}{2}} \frac{1}{e^{\frac{h\nu}{kT_{ast}}} - 1} \cos^2(\phi) \cos(\theta - \alpha) d\theta d\phi \right] \quad (3)$$

where

$$T_{ast} = \left[\frac{(1 - A)S_\odot}{r_h \eta \epsilon \sigma_{SB}} \right]^{\frac{1}{4}} (\cos\phi)^{\frac{1}{4}} (\cos\theta)^{\frac{1}{4}}. \quad (4)$$

The terms $F_{reflected}$ and $F_{thermal}$ are the observed V -band and IRAC 8.0 μm band fluxes ($\text{W m}^{-2} \text{Hz}$) respectively. Variables in the equation for reflected flux are: ν is the frequency of observation, in this case V -band, R_{\odot} and T_{\odot} are the radius (m) and temperature (K) of the Sun, r is the asteroid heliocentric distance in meters, D is the asteroid diameter in meters and Δ is the asteroid geocentric distance, p_v is the geometric albedo of the asteroid in V -band, R is the relative reflectance of the asteroid as measured with respect to the V -band reflectance and $\tilde{\alpha}$ is the observed phase angle in radians. Other variables in the equation for thermal flux are: $d_{Spitzer}$ is the asteroid-*Spitzer* separation (AU), ϵ is the asteroid emissivity which is assumed to be 0.9, A is the Bond Albedo, S_{\odot} is the solar constant, r_h is the asteroid heliocentric distance in AU, and η is the beaming parameter. Adopting mean values for the known asteroids in our datasets $r_h = 2.82$ AU, $\delta = 1.89$ AU (optical) and $r_h = 2.68$ AU, $d_{Spitzer} = 2.28$ AU, (*Spitzer* asteroids; Table 6), assuming $\eta = 1$ with $p_v = 0.15$ and $\cos(\tilde{\alpha}) = 0.99$, the minimum asteroid radii detected in our data are $\simeq 1020$ m in the optical and $\simeq 450$ m in the IRAC 8.0 μm channel. Although *Spitzer* is far more efficient than optical imaging surveys at detecting smaller asteroids, asteroids identified from these two data sets comprise a set of bodies with similar size ranges within the main belt.

The IR and optical data can be used to obtain the power law size-frequency distribution at 3 similar latitudes. In both the optical and the mid-IR, flux can be used as a proxy for size in obtaining the size-frequency distribution assuming that the Bond albedo is well behaved as a function of wavelength. By adopting a power law distribution for the surface density distribution $\propto f^{-\alpha}$, we use the completeness corrected counts to measure the power law slopes summarized in Table 7. The derived optical and IR slopes are similar at all latitudes within the uncertainties, with a mean value of $\alpha = -0.111 \pm 0.077$ for the surface density distribution of asteroids. However, the formal errors suggest that the optical data provides a better constraint on α . Our derived α -values (Table 7) for the *Spitzer* fields differs somewhat from those cited by Meadows et al. (2004). The differences can be attributed to how the asteroid photometry was conducted; Meadows et al. (2004) employed PSF-fitting (using, at that time, a poorly determined IRAC PSF), whereas we resort to aperture photometry to measure the flux density. In addition, differences in completeness also lead to variances in our results as opposed to those presented in Meadows et al. (2004). We cite 80% completeness at 100 μJys for moving-objects, while Meadows et al. (2004) quote 90% completeness at the same flux level for point sources.

As the derived slopes of the surface density distributions are similar at optical wavelengths, we employed a Kolmogorov-Smirnov (KS) test using the mean rates of motion of the asteroids at 0° and 15° ecliptic latitude to discriminate whether these bodies detected in the optical fields are drawn from the same size and magnitude population distributions. Unlike a χ^2 test, data is not binned in the KS test and the KS test can be used on data

sets of different lengths. Due to the low number of asteroids detected in the 10° and 15° , binning of the data was rejected due to the associated loss of information and arbitrariness of defining bin sizes. The derived probability is 96.88%, strongly suggesting that the two fields represent the same distance (rate) population. Similarly, a KS test to determine the likelihood that the asteroids represent the same size distribution yields only a 41.32% probability that the objects at 15° represent the same size distribution as those detected at 0° ecliptic latitude. This statistical inference suggests that the size distribution of asteroids at 0° and 15° are dissimilar; however, the veracity of this conclusion is limited by small number detection statistics of our data. Table 8 summarizes our probability analysis of the magnitude distribution (e.g., asteroid diameters) as a function of ecliptic latitude compared to the 0° field. Lastly, although the KS test indicates that the 0° and 15° optical fields are likely not the same population, they do appear to follow a distribution in which large, thus bright, objects are rare, whereas small and thus faint, objects are more numerous.

3.3. Comparison to models

Our observed asteroid frequency distribution can be juxtaposed with current models describing the evolution of the asteroid populations in the solar system, such as the Statistical Asteroid Model (SAM) developed by Tedesco, Cellino, & Zappalá (2005). The SAM uses a set of 8603 asteroids with absolute magnitudes less than 15.75 (asteroids with diameters of $\gtrsim 2.5$ km) to determine a size-frequency distribution of asteroids which is assumed to be smooth to diameters of 1 km. This model also incorporates an albedo distribution derived from 15 dynamical families and 3 “background” populations based on 1980 asteroids which have diameter and albedo determinations from MSX (Tedesco, Egan, & Price 2002) and IRAS (Veeder & Tedesco 1992; Tedesco et al. 2002). A number of asteroids are excluded from this model, including those with inclinations greater than 25° , those with eccentricities > 0.3 .

The asteroid number counts observed with both *Spitzer* and the LBT are less than those predicted by the SAM. For a limiting flux of 0.06 mJy at $8 \mu\text{m}$ the SAM predicts 430 ± 40 asteroids at 0° latitude and 250 ± 20 asteroids at 5° latitude. One reason the SAM may overestimate the number of asteroids is the assumed faint flux limit of Tedesco, Cellino, & Zappalá (2005) which corresponds to an effective diameter of 0.6 km. This flux limit is fainter than the completeness for both fields, thus the SAM over predicts the number of small asteroids which would be observed by *Spitzer*. The overestimate of the number of asteroids may also be due to a fundamental assumption of the SAM – the power law slope of the size-frequency distribution is continuous to diameters less than 1 km. This is not observed in the optical.

The size-frequency distribution appears to fall off around 3 km (Jedicke & Metcalfe 1998); however, the reasons for this fall off are not well understood. Two possible reasons for the fall off in observed data are: 1) the bright limiting magnitude of most asteroid surveys excludes detections of asteroids smaller than 1 km in diameter, or 2) the asteroids smaller than 1 km may not be solid, but may instead be easily disruptible piles of rubble. If the predicted number of asteroids is scaled from the SAM with a model that yields the number of asteroids with diameters > 0.6 km being 2.4 times the number of asteroids with diameters > 1.0 km, the SAM still predicts 179 ± 17 asteroids in the 0° latitude field and 104 ± 8 asteroids in the 5° latitude field. The estimate at the high latitude is nearly in agreement with our FLS results; however, the SAM still overestimates the number of asteroids in the 0° field. The latter discrepancy may be due to asteroids with high albedos (> 0.25) which are not detected in the IRAC channels because they are too cool and thus their thermal fluxes are below the detection thresholds in this data.

For the LBT data which has limiting diameters of ~ 2 km, the number counts are within the uncertainty of the SAM prediction. For the SDSS survey which has a point source completeness limit of $V = 22.2$, the SAM predicts 115 ± 10 asteroids at 0° latitude and 75 ± 5 asteroids at 5° latitude. This completeness limit is fainter than ours by 0.9 mag; however, the model values are nearly in agreement with the asteroid number counts at these two latitudes. Unfortunately, the SAM does not predict asteroid counts at higher latitudes ($\beta > 5^\circ$) and the current version of the SAM only uses asteroids with inclinations less than 20° to make estimates on number counts. A subset of our newly detected asteroids have large inclinations. In fact this limitation of the SAM complicates derivation of the size-frequency distribution and physical characteristics of well known and well characterized targets such as Pallas and asteroid dynamical groups such as Hungarias and Phocaeas (Carvano et al. 2001).

3.4. Asteroid Diameters, Albedos, and Colors

Direct comparison of mean and median IRAC $8.0 \mu\text{m}$ fluxes (§2.2) of asteroids in the two FLS fields and the SWIRE field, reveals that the SWIRE asteroids are, on average across the population, brighter than those asteroids at 0° and 5° latitude detected in the FLS fields, by a factor of two. This variance in brightness could be explained as a difference in asteroid diameter assuming that the populations have comparable albedos. We explored this possibility by estimating the diameters and deriving albedos for all asteroids which were detected in all four IRAC bands using the Near Earth Asteroid Thermal Model (NEATM; Delbo & Harris 2002; Delbo 2004). In this model, the thermal flux is dependent upon the

sub-solar temperature and the temperature distribution of the surface of the asteroid. The latter is solely dependent on the albedo and η as model variables. Thus, our implementation of NEATM follows the Delbo & Harris (2002) and Delbo (2004) prescription whereby the model fits the IR fluxes and the optical absolute magnitude of asteroids (H) by varying the geometric albedo (through a χ^2 -minimization) until a best fit is found. The *Spitzer* fluxes were first color-corrected according to the prescription described in the IRAC Data Handbook (Spitzer Science Center 2006), resulting in the measured fluxes being divided by 1.1717 and 1.1215 at 5.8 μm and 8.0 μm , respectively. The asteroid diameter is then calculated by the relation of Fowler & Chillemi (1992) which uses only the geometric albedo and the absolute magnitude as input values. Because IRAC asteroid spectral energy distributions are composites of both thermal emission and reflected solar light (e.g., Mueller, Harris, & Fitzsimmons 2007), we derived albedo and diameter estimates of the asteroids using only data from IRAC channels 3 and 4. From the channel 3 and 4 fits, we find that the percentage of reflected solar light in our channel 1 photometry to be $\simeq 56\%$ and $\simeq 14\%$ in the channel 2 photometry. Our modeling results for *known* asteroids detected in our IRAC fields are summarized in Table 6. The mean diameters of asteroids in SWIRE is 5.91 km while the mean asteroid diameter in the FLS is 2.28 km.

Analysis of the mean geometric albedos and derived sizes for these objects suggests they divide between the two populations. The mean geometric albedo for asteroids in the FLS fields is 0.24 ± 0.07 as opposed to 0.10 ± 0.05 for asteroids in the SWIRE fields. No low albedo asteroids ($p_V \lesssim 0.1$) were detected in the *Spitzer* FLS fields, whereas in the SWIRE fields they are frequent. Evidently the surface composition of the asteroids in the SWIRE fields contains more carbonaceous material than the asteroids in the FLS, as carbonaceous chondrites have significantly lower albedos in the 0.03 to 0.11 range (Gaffey 1976; Johnson & Fanale 1973).

However, the marked dichotomy in derived albedos is most likely a result of the two *Spitzer* surveys sampling different asteroid taxonomy classes within the general asteroid belt. An extensive analysis of $\sim 88,0000$ objects in the Sloan Digital Sky Survey Moving Object Catalog (SDSS MOC) 4 by Parker et al. (2008) demonstrates that there is a strong correlation between SDSS color, asteroid taxonomy (C-, S-, V-type), and orbital elements. In Fig. 3 we plot the proper orbital elements a (orbital semi-major axis) vs. i (orbital inclination) of our SWIRE (green squares) and FLS (red triangles) detected asteroids overlaid on 207,942 numbered asteroids (black dots) with orbital elements in the ASTORB files (Bowell 2001). The location of the major Kirkwood gaps as defined by Parker et al. (2008) are indicated, and the colored symbols used to identify the *Spitzer*-detected asteroids are coded by derived albedo. Open symbols are for *Spitzer* asteroids with derived albedos, $p_V \lesssim 0.1$, while filled symbols identify asteroids with $p_V > 0.1$. The majority ($\simeq 80\%$) of

the low albedo asteroids detected in the *Spitzer* data reside at high inclination in the outer belt. Primitive asteroids, with C-type colors and generally low albedos ($p_V < 0.1$), are seen to dominate the asteroid population in the outer belt, while S-type asteroids with p_V ranging from ~ 0.15 to 0.2 tend to be more dominant in the middle and inner asteroid belt (Parker et al. 2008). Our SWIRE data clearly samples asteroids in the middle and outer belts, and in fact, for the first time, we are able to estimate the albedos of km-sized asteroids in the outer belt (Table 6).

The low albedos ($p_V \lesssim 0.1$) of the $\simeq 6$ km-sized outer belt SWIRE asteroids are similar to the albedos derived for Jupiter-family comets, $0.02 \lesssim p_V \lesssim 0.06$ (Fernández et al. 2008; Lamy et al. 2004). Recent modeling by Levison et al. (2008) investigating the capture likelihood of cometary planetesimals into the asteroid belt (leading the establishment of a D-type population) suggests that the inner edge of the D-type population is near $a \sim 2.6$ AU. Whether the population of low albedo asteroids discovered in our SWIRE fields discussed here are organic-rich, primitive objects can only be verified with follow-up spectroscopy.

From flux measurements in all 4 IRAC channels, we can also begin to constrain the colors of asteroids. This is beneficial for both the understanding of bulk asteroid albedo variations as a function of size and other orbital parameters such as orbital semi-major axis or inclination and for the future exclusion of asteroids from galactic or extragalactic catalogs. Figure 4 is an adaptation of the work by Lacy et al. (2004) which shows the IRAC colors of fixed astronomical objects where we have now included asteroid color data derived from the our FLS and SWIRE field photometry. Asteroids mainly reside in one isolated locus in color space. The size of this locus is dependent upon both temperature and albedo. The shortest wavelength observations with IRAC at $3.6 \mu\text{m}$ trace the fraction of reflected incident solar flux, thus traces albedo, while the $8.0 \mu\text{m}$ to $4.5 \mu\text{m}$ ratio traces the thermal emission and thus the albedo and distance of an asteroid.

4. CONCLUSION

Our combined optical survey of $\simeq 0.96$ square degrees and *Spitzer* IRAC $8.0 \mu\text{m}$ fields encompassing from 0.26 to $\simeq 9.1$ square degrees of sky at five latitudes perpendicular to the ecliptic plane resulted in detection of 118 main belt asteroids, of which 91 are newly identified objects either at optical or infrared wavelengths. The optical and mid-IR asteroid counts and fluxes demonstrate that the slope of the size-frequency distribution is consistent with that of a similar size population at 0° and 15° ecliptic latitude. The derived power law slopes of the asteroid surface density distribution are similar at within each $\sim 5^\circ$ ecliptic latitude bin with a mean slope of -0.111 ± 0.077 . The observed asteroid number densities at

optical wavelengths are generally consistent with those derived from the Standard Asteroid Model within the ecliptic plane. However, we find an over density at $\beta \gtrsim 5^\circ$ in our optical fields, while the infrared number densities are under dense by factors of 2 to 3 at all ecliptic latitudes.

For the 28 known asteroids detected in all four IRAC channels, mean albedos range from 0.24 ± 0.07 to 0.10 ± 0.05 , statistically suggesting that these are two different populations. Our SWIRE data clearly samples low albedo asteroids in the middle and outer belts, and in fact, for the first time, we are able to estimate the albedos of km-sized asteroids in the outer belt.

In order to increase our number statistics and lower the errors, we are completing the data-mining of additional, extant multi-epoch survey *Spitzer* IRAC and MIPS dataset and are undertaking complimentary ground based optical observations with the LBT and the 2.3-m Bok Telescope at Kitt Peak. These data will provide a survey area more than 3 times larger than that described in this manuscript and will also expand analysis of asteroid number counts to ecliptic latitudes of 20° .

The errors in the slope of the size-frequency distribution cannot be decreased by greater number statistics alone. The use of fluxes as proxies for asteroid sizes does not account for variations in albedo; therefore, additional mid-IR data is required to obtain albedos and sizes for a large number of asteroids. We in the process of completing the data-mining of additional, extant multi-epoch survey *Spitzer* IRAC and MIPS dataset while undertaking complimentary ground based optical observations with the LBT and the 2.3-m Bok Telescope at Kitt Peak in order to increase our number statistics and lower the completeness statistics uncertainties. These data will provide a ecliptic survey area more than 3 times larger than that described in this manuscript and will also expand analysis of asteroid number counts to ecliptic latitudes of 20° . These data will extend the number of asteroids with accurate sizes to diameters much smaller than the 10 km IRAS detection limit enabling reliable number counts for asteroids with diameters $\lesssim 1$ km and assessment of whether the fall off in the size-frequency distribution of main belt asteroids distribution with diameters $\lesssim 1$ km is a real signature, or an artifact introduced by the limiting magnitudes of current asteroids surveys.

This work is based on observations made with the *Spitzer* Space Telescope, which is operated by the Jet Propulsion Laboratory, California Institute of Technology under a contract with NASA. Support for this work was provided by NASA through an award issued by JPL/Caltech. Support for this work also was provided by NASA through contracts 1263741, 1256406, and 1215746 issued by JPL/Caltech to the University of Minnesota. E.R. and C.E.W. also acknowledge support from the National Science Foundation grant AST-0706980.

This work is also based on data acquired using the Large Binocular Telescope (LBT). The LBT is an international collaboration among institutions in the United States, Italy and Germany. LBT Corporation partners are: The University of Arizona on behalf of the Arizona University system; Istituto Nazionale di Astrophysica, Italy; LBT Beteiligungsgesellschaft, Germany, representing the Max-Planck Society, the Astrophysical Institute Potsdam, and Heidelberg University; The Ohio State University, and The Research Corporation, on behalf of The University of Notre Dame, University of Minnesota, and University of Virginia. The authors also acknowledge the detailed and very helpful comments of anonymous referees whose insights greatly improved the manuscript.

Facilities: Spitzer (IRAC, MIPS) LBTO (LBC 4048 CCD)

REFERENCES

- Abazajian, K., et al. 2004, *AJ*, 128, 502
- Bottke, Jr., W. F., Durda, D. D., Nesvorny, D., Jedicke, R., Morbidelli, A., Vokrouhlicky, D., & Levison, H. 2005, *Icarus*, 175, 111
- Bowell, E. 2001, *ASTROORB*, Lowell Obs., Flagstaff, AZ
- Carvano, J. M., et al. 2001, *Icarus*, 149, 173
- Delbo, M. 2004, Ph.D. Thesis, Freie Universtat Berlin
- Delbo, M., & Harris, A. W. 2002, *M&PS*, 37, 1929
- Fazio, G. G., et al. 2004, *ApJS*, 154, 10
- Fernández, Y. R., et al. 2008, in *Asteroids, Comets, Meteors*, 2008LPICo1405.8307F
- Fowler, J. W., & Chillemi, J. R. 1992, in *IRAS Minor Planet Survey*, eds. E. F. Tedesco (Phillips Lab. Tech. Rep. PL-TR-92-2049) (Hanscom AFB, MA: Phillips Lab., Dir. Geophys., Air Force Mater. Command), 17
- Gaffey, M. 1976, *JGR*, 81, 905
- Gehrz, R. D., et al. 2007, *Rev. Sci. Instrum.*, 78, 011302.
- Giallongo, E., Ragazzoni, R., Grazian, A., et al. 2008, *A&A*, 482, 349
- Hill, J. M., Green, R. F., & Slagle, J. H. 2006, *Proceedings of the SPIE*, 6267, 31
- Ivezić, Ž., et al. 2001, *AJ*, 122, 2749
- Jedicke, R., & Metcalfe, T. S. 1998, *Icarus*, 131, 245
- Johnson, T. V., & Fanale, F. P. 1973, *JGR*, 78, 8507
- Joye, W. A., & Mandel, E. 2003, *ASPC*, 295, 489
- Kaiser, N., 2004, *Proceedings of the SPIE*, 5489, 11
- Lacy, M. D., et al. 2003, *ApJS*, 154, 166
- Lamy, P. L., Toth, I., Fernández, Y. R., & Weaver, H. A. 2004, in *Comets II*, eds. M. Festou, H. Keller, and A. Weaver (Tucson, AZ: Univ. Arizona Press), 223

- Lebosfsky, L. A. & Spencer, J. R. 1989, in Asteroids II (A90-27001 10-91), (University of Arizona Press: Tucson, AZ), p.128
- Levison, H. F., Bottke, W. F., & Nesvorný, D. 2008, in Asteroids, Comets, Meteors, 2008LPICo1405.8156L
- Lonsdale, C. J., et al. 2004, ApJS, 154, 54
- Lonsdale, C. J., et al. 2003, PASP, 115, 897
- Meadows, V. S., et al. 2004, ApJS, 154, 469
- Mueller, M., Harris, A. W., & Fitzsimmons, A. 2007, Icarus, 187, 611
- Parker, A., Ivezić, Ž., Jurić, M., Lupton, R., Sekora, M. D., & Kowalski, A. 2008, Icarus, 198, 138
- O'Brien, D., & Greenberg, R. 2005 Icarus, 178, 179
- Ragazzoni, R., et al. 2006 Proceedings of the SPIE, 6267, 33
- Rieke, G. H., et al. 2004 ApJS, 154, 25
- Ryan, E. L., & Woodward, C. E. 2006, American Astron. Soc., DPS meeting #38, #59.14, 2006DPS38.5914R
- Stapelfeldt, K. R., et al. 2006, American Astron. Soc., DPS meeting #38, #58.06, 2006DPS38.5806S
- Spitzer Science Center 2006, Infrared Array Camera Data Handbook V3.0 (Pasadena: SSC), <http://ssc.spitzer.caltech.edu/irac/dh/>
- Tedesco, E. F., & Desert, F. X. 2002, ApJ, 123, 2070
- Tedesco, E. F., Egan, M. P., & Price, S. D. 2002, AJ, 124, 583
- Tedesco, E. F., et al. 2002, AJ, 123, 1056
- Tedesco, E. F., Cellino, A., & Zappalá, V. 2005, AJ, 129, 2869
- Trilling, D. E., Mueller, M., Hora, J. L., Fazio, G., Spahr, T., Stansberry, J. A., Smith, H. A., Chesley, S. R., & Mainzer, A. K. 2008, ApJ, 683, L199
- Veeder, G. J., & Tedesco, E. F. 1992, in IRAS Minor Planet Survey, eds. E. F. Tedesco (Phillips Lab. Tech. Rep. PL-TR-92-2049) (Hanscom AFB, MA: Phillips Lab., Dir. Geophys., Air Force Mater. Command), 107

Werner, M. W., et al. 2004, ApJS, 154, 1

Wetherill, G. W., 1989, in Asteroids II (A90-27001 10-91), (University of Arizona Press: Tucson), p.661

Zacharias, N., et al. 2004, AJ, 127, 3043

Table 1. LBT/LBC OBSERVATIONAL SUMMARY

Pointing Name	Field Center RA (J2000)	Field Center Dec (J2000)	Date (2007 UT)	Time (UT)	Seeing ($''$)	Zero-point Offset (mag)
<u>0 degree field, pointing 1</u>						
Epoch 1	6:14:21.68	+23:25:15.49	Jan 16	07:55:20	2.13	7.37 \pm 0.10
Epoch 2	6:14:21.68	+23:25:15.49	Jan 16	08:00:01	2.74	7.50 \pm 0.11
Epoch 3	6:14:21.68	+23:25:15.49	Jan 16	09:51:30	2.52	7.40 \pm 0.13
<u>0 degree field, pointing 2</u>						
Epoch 1	6:14:22.33	+23:40:18.72	Jan 16	08:01:21	2.19	7.68 \pm 0.11
Epoch 2	6:14:22.33	+23:40:18.72	Jan 16	09:13:54	2.67	7.81 \pm 0.06
Epoch 3	6:14:22.33	+23:40:18.72	Jan 16	09:57:22	2.67	7.78 \pm 0.06
<u>5 degree field, pointing 1</u>						
Epoch 1	6:14:56.16	+28:25:17.94	Jan 25	02:49:41	1.50	7.43 \pm 0.04
Epoch 2	6:14:56.16	+28:25:17.94	Jan 25	03:49:01	1.64	7.47 \pm 0.04
Epoch 3	6:14:56.16	+28:25:17.94	Jan 25	06:39:50	2.20	7.66 \pm 0.04
<u>5 degree field, pointing 2</u>						
Epoch 1	6:14:56.78	+28:40:19.50	Jan 25	02:55:22	1.50	7.48 \pm 0.04
Epoch 2	6:14:56.78	+28:40:19.50	Jan 25	03:54:47	1.75	7.56 \pm 0.04
Epoch 3	6:14:56.78	+28:40:19.50	Jan 25	06:45:37	1.71	7.66 \pm 0.04
<u>10 degree field, pointing 1</u>						
Epoch 1	6:15:33.49	+33:25:15.14	Jan 24	02:17:27	1.44	7.36 \pm 0.03
Epoch 2	6:15:33.49	+33:25:15.14	Jan 24	04:34:49	2.12	7.62 \pm 0.03

Table 1—Continued

Pointing Name	Field Center RA (J2000)	Field Center Dec (J2000)	Date (2007 UT)	Time (UT)	Seeing (")	Zero-point Offset (mag)
Epoch 3 <u>10 degree field, pointing 2</u>	6:15:33.49	+33:25:15.14	Jan 24	08:10:00	2.64	7.67±0.03
Epoch 1	6:15:34.08	+ 33:40:19.96	Jan 24	02:23:01	1.44	7.33±0.03
Epoch 2	6:15:34.08	+ 33:40:19.96	Jan 24	04:40:57	2.16	7.55±0.03
Epoch 3	6:15:34.08	+ 33:40:19.96	Jan 24	08:15:42	2.65	7.55±0.03
<u>15 degree field, pointing 1</u>						
Epoch 1	6:16:17.02	+38:25:09.47	Jan 24	02:05:07	1.35	7.35±0.03
Epoch 2	6:16:17.02	+38:25:09.47	Jan 24	04:13:06	1.79	7.60±0.02
Epoch 3	6:16:17.02	+38:25:09.47	Jan 24	07:47:27	2.62	7.68±0.03
<u>15 degree field, pointing 2</u>						
Epoch 1	6:16:15.22	+38:40:11.62	Jan 24	02:10:49	1.28	7.24±0.03
Epoch 2	6:16:15.22	+38:40:11.62	Jan 24	04:19:06	2.25	7.60±0.03
Epoch 3	6:16:15.22	+38:40:11.62	Jan 24	07:54:28	3.08	7.64±0.03

Table 2. SUMMARY OF ASTEROID DETECTIONS BY LATITUDE AND NUMBER COUNT STATISTICS

Field Ecliptic Latitude	Number Asteroids Detected	Number Asteroids Per Square Degree ^a	Total Number Asteroids Per Square Degree ^b	Limiting Magnitude or Flux
LBT <i>V</i> -Band				
0°	24	85	91± 10	22.3
5°	21	74	80± 9	22.0
10°	11	39	41± 6	22.2
15°	6	21	23± 5	22.2
FLS IRAC 8μm				
0°	24	85	91± 10	25.7 μJy
5°	21	74	80± 9	25.7 μJy
SWIRE IRAC 8μm				
–17°	11	39	41± 6	35.4 μJy

^aDirectly calculated from the number of asteroids detected where each LBT field covers 0.24 square degrees of sky, the FLS fields are 0.13 square degrees, and the single SWIRE field is 9.1 square degrees in extent.

^bNumber of asteroids including completeness.

Table 3. OPTICALLY DETECTED ASTEROIDS – MACHINE READABLE TABLE^a

Asteroid Name	Discovery Flag	Year	Month	Day (UT)	RA ^a (hrs)	RA (min)	RA (sec)	Dec ^b (degr)	Dec (min)	Dec (sec)	Mag	Mag Error	Filter
sdt01	1	2007	01	16.33147	06	14	03.68	+23	21	03.0	19.72	0.03	V
sdt01	1	2007	01	16.38195	06	14	01.21	+23	21	08.7	20.34	0.04	V
sdt01	1	2007	01	16.41215	06	13	59.70	+23	21	12.1	20.16	0.04	V
sdt02	1	2007	01	16.33147	06	13	56.23	+23	15	27.2	20.94	0.13	V
sdt02	1	2007	01	16.38195	06	13	53.82	+23	15	26.8	21.54	0.10	V
sdt02	1	2007	01	16.41215	06	13	52.35	+23	15	27.0	21.46	0.04	V
:													

^aFull catalog available on-line.

^bRA and Declination given in J2000 coordinates.

Table 4. SPITZER DETECTED ASTEROIDS – MACHINE READABLE TABLE^{a,b}

Asteroid Name	PID	AOR Key	YR	MN	Day (UT)	Hr	Min	Sec	RA J2000 (°)	Dec J2000 (°)	Ecliptic Long (°)	Ecliptic Lat (°)	F _{3.6} (μ Jy)	F _{3.6} ^{err} (μ Jy)	F _{4.5} (μ Jy)	F _{4.5} ^{err} (μ Jy)	F _{5.8} (μ Jy)	F _{5.8} ^{err} (μ Jy)	F _{8.0} (μ Jy)	F _{8.0} ^{err} (μ Jy)
2001QY160	98	6095104	2004	01	21	02	35	25.728	181.0084	-0.0412	180.9416	0.3633	89.4	8.1	18.9	14.4	95.7	45.7	939.9	179.4
0h	98	6095104	2004	01	21	02	35	25.728	181.0051	-0.1183	180.9693	0.2913	2.3	2.2	7.7	6.9	65.3	35.5	548.8	132.8
2004BS160	98	6095104	2004	01	21	02	35	25.728	181.0004	-0.1816	180.9902	0.2313	3.7	3.6	1.7	1.7	52.5	52.2	103.2	49.2
2000AX136	98	6095104	2004	01	21	02	35	25.728	180.9245	-0.1815	180.9204	0.2012	4.8	4.6	103.7	47.2	240.9	79.9	2526.7	305.6
:																				
:																				

^aFull catalog available on-line.

^bObserved fluxes, no IRAC color-correction applied.

Table 5. OBSERVED ASTEROID IRAC FLUXES^a

Provisional Designation	F _{3.6} (μ Jy)	F _{4.5} (μ Jy)	F _{5.8} (μ Jy)	F _{8.0} (μ Jy)
SWIRE Asteroids				
2004TH222	18.5 \pm 14.1	53.6 \pm 30.6	241.0 \pm 80.3	1682.6 \pm 246.3
2005YV181	6.0 \pm 5.6	16.23 \pm 12.8	128.4 \pm 55.2	933.8 \pm 179.0
2005YV50	16.7 \pm 14.2	15.7 \pm 12.4	64.5 \pm 36.0	570.6 \pm 136.2
1999WA1	45.1 \pm 27.1	113.4 \pm 50.0	938.5 \pm 172.8	7314.0 \pm 532.0
2004TO8	109.2 \pm 48.7	259.0 \pm 82.6	1684.4 \pm 237.5	10301.9 \pm 634.3
2006AP1	5.8 \pm 5.4	32.8 \pm 21.7	263.8 \pm 84.7	1677.9 \pm 245.7
2005WX162	10.4 \pm 8.9	38.0 \pm 24.1	311.5 \pm 93.5	2287.0 \pm 290.30
1999VY171	75.7 \pm 38.5	383.9 \pm 103.8	2867.7 \pm 314.2	18500.5 \pm 856.9
1999JZ7	4.0 \pm 4.9	25.5 \pm 18.1	196.8 \pm 71.2	1512.8 \pm 232.3
2000VP1	15.9 \pm 12.7	25.0 \pm 17.8	113.9 \pm 51.2	775.1 \pm 161.3
2005YH117	6.7 \pm 6.2	48.0 \pm 28.4	470.0 \pm 118.0	3570.0 \pm 366.2
2002FE15	12.0 \pm 10.1	47.9 \pm 28.4	355.7 \pm 100.8	4308.9 \pm 403.4
2005YX74	83.1 \pm 42.7	118.5 \pm 52.0	538.9 \pm 127.5	4465.2 \pm 411.6
2002CN96	15.5 \pm 12.3	65.0 \pm 35.3	584.1 \pm 133.3	3106.3 \pm 343.6
FLS Asteroids				
2001QY160 ^b	8.9 \pm 7.8	31.8 \pm 22.6	101.3 \pm 47.5	905.4 \pm 175.8

Table 5—Continued

Provisional Designation	F _{3.6} (μ Jy)	F _{4.5} (μ Jy)	F _{5.8} (μ Jy)	F _{8.0} (μ Jy)
2000AX136 ^b	114.8±50.4	217.6± 74.2	1228.2± 200.3	8993.1± 593.3
2004BH160	9.1± 9.3	11.4± 10.9	11.5± 11.7	73.6± 39.6
2001QD49 ^b	7.1± 7.4	11.2± 12.2	16.1± 16.0	109.9± 51.3
2002WL7 ^b	18.2± 13.9	50.0± 29.1	497.6± 121.4	3239.4± 347.8
1999FZ24 ^b	41.7± 25.9	45.2± 27.3	211.0± 74.1	2116.3± 277.6
2001RP137 ^b	8.3± 7.6	14.3± 14.2	34.9± 24.1	273.5± 89.2
2004EU91	9.3± 9.2	7.2± 6.8	35.7± 26.5	116.5± 53.3
2004CA105	61.7± 35.8	54.6± 33.7	59.9± 34.8	487.4± 124.5
2002RG106	12.2± 10.4	5.3± 5.3	22.9± 17.6	228.3± 80.5
2004BU99	6.3± 5.8	7.9± 7.4	40.3± 25.9	398.9± 110.9
2004BS160	8.1± 8.6	3.1± 3.1	21.4± 30.7	101.9± 49.0
2001SB182	14.1± 11.9	11.8± 11.0	32.6± 22.6	184.0± 70.1
2004FG8	6.1± 7.2	7.7± 7.0	25.5± 19.2	185.5± 70.7

^aObserved fluxes, no IRAC color-correction applied.

^bAsteroids also reported in Meadows et al. (2004).

Table 6. STANDARD THERMAL (NEATM) MODEL DERIVED ASTEROID DIAMETERS AND ALBEDOS

Provisional Designation	Heliocentric ^a Distance (AU)	Spitzer ^a Distance (AU)	Phase Angle (°)	Absolute ^b Magnitude (H)	NEATM Diameter (km)	Geometric Albedo	Beaming parameter	Model χ^2
SWIRE Asteroids								
2004 TH222	2.08	1.79	29.4	15.4	2.83	0.14	1.69	0.0002
2005 YV181	3.27	3.09	18.20	15.5	3.91	0.07	0.79	0.0157
2005 YV50	2.38	2.14	25.36	16.0	2.45	0.12	1.66	0.0087
1999 WA1	2.82	2.60	21.25	12.7	9.16	0.18	1.01	0.0225
2004 TO8	2.66	2.44	22.57	14.5	9.02	0.03	1.04	0.5826
2006 AP1	2.91	2.71	20.53	15.5	3.59	0.09	0.77	0.0035
2005 WX162	2.83	2.61	21.20	15.3	5.10	0.05	1.03	0.0141
1999 VY171	2.56	2.34	23.48	14.0	10.92	0.04	1.04	0.6644
1999 JZ7	2.33	2.08	26.02	14.0	3.39	0.39	1.35	0.0308
2000 VP1	2.43	2.21	24.83	15.7	1.99	0.23	1.03	0.0143
2005 YH117	2.91	2.73	20.57	15.4	6.73	0.03	1.01	0.0161
2002 FE15	3.39	3.25	17.54	14.5	12.41	0.02	1.05	0.3090
2005 YX74	2.85	2.64	20.99	14.8	5.35	0.08	1.05	0.0859
2002 CN96	2.95	2.74	20.29	14.8	5.88	0.06	0.87	0.9232
FLS Asteroids								
2001 QY160	2.96	2.39	17.74	15.0	3.26	0.17	1.02	0.0241

Table 6—Continued

Provisional Designation	Heliocentric ^a Distance (AU)	Spitzer ^a Distance (AU)	Phase Angle (°)	Absolute ^b Magnitude (H)	NEATM Diameter (km)	Geometric Albedo	Beaming parameter	Model χ^2
2000 AX136	2.40	1.80	22.02	13.1	6.89	0.21	1.33	0.0002
2004 BH160	2.42	1.82	21.86	18.4	0.51	0.30	1.03	0.0001
2001 QD49	2.77	2.19	18.98	17.5	0.94	0.20	1.00	0.0048
2002 WL7	2.69	2.11	19.55	15.3	4.48	0.07	1.05	0.1406
1999 FZ24	3.10	2.53	16.93	13.8	5.81	0.16	1.03	0.1115
2001 RP137	2.93	2.36	17.90	16.7	1.72	0.13	1.02	0.0012
2004 EU91	2.40	1.80	22.04	18.1	0.51	0.39	0.76	0.1778
2004 CA105	2.80	2.22	18.77	14.7	2.27	0.44	1.03	0.0062
2002 RG106	2.69	2.10	19.58	16.1	1.30	0.38	1.045	0.108
2004 BU99	2.17	1.54	24.53	17.4	1.84	0.06	2.50	0.0008
2004BS160	2.41	1.81	21.99	18.6	0.57	0.20	1.01	0.0178
2001SB182	3.02	2.46	17.36	15.6	1.39	0.53	0.75	0.0636
2004FG8	2.01	1.37	26.61	18.5	0.74	0.13	1.90	0.0001

^aHeliocentric, r_h , and *Spitzer*-asteroid distances at epoch of observation.

^bAbsolute Magnitudes are values given in the JPL Horizons database, <http://ssd.jpl.nasa.gov/?horizons>.

Table 7. POWER LAW SLOPES OF THE SURFACE DENSITY DISTRIBUTIONS

Dataset	Bandpass	Ecliptic Latitude	Slope α
LBT	V	0°	-0.118 ± 0.070
LBT	V	5°	-0.161 ± 0.074
LBT	V	15°	-0.131 ± 0.093
FLS	IRAC $8\mu\text{m}$	0°	-0.083 ± 0.145
FLS	IRAC $8\mu\text{m}$	5°	-0.100 ± 0.240
SWIRE	IRAC $8\mu\text{m}$	-17°	-0.075 ± 0.340

Table 8. ASTEROID POPULATION PROBABILITIES, MEAN AND MEDIAN MAGNITUDES

Field Ecliptic			
Latitude (°)	Probability ^a (%)	Median (mag)	Mean (mag)
0	100	20.6	20.45
5	66.24	20.5	20.41
10	38.89	19.8	20.00
15	41.32	20.8	20.65

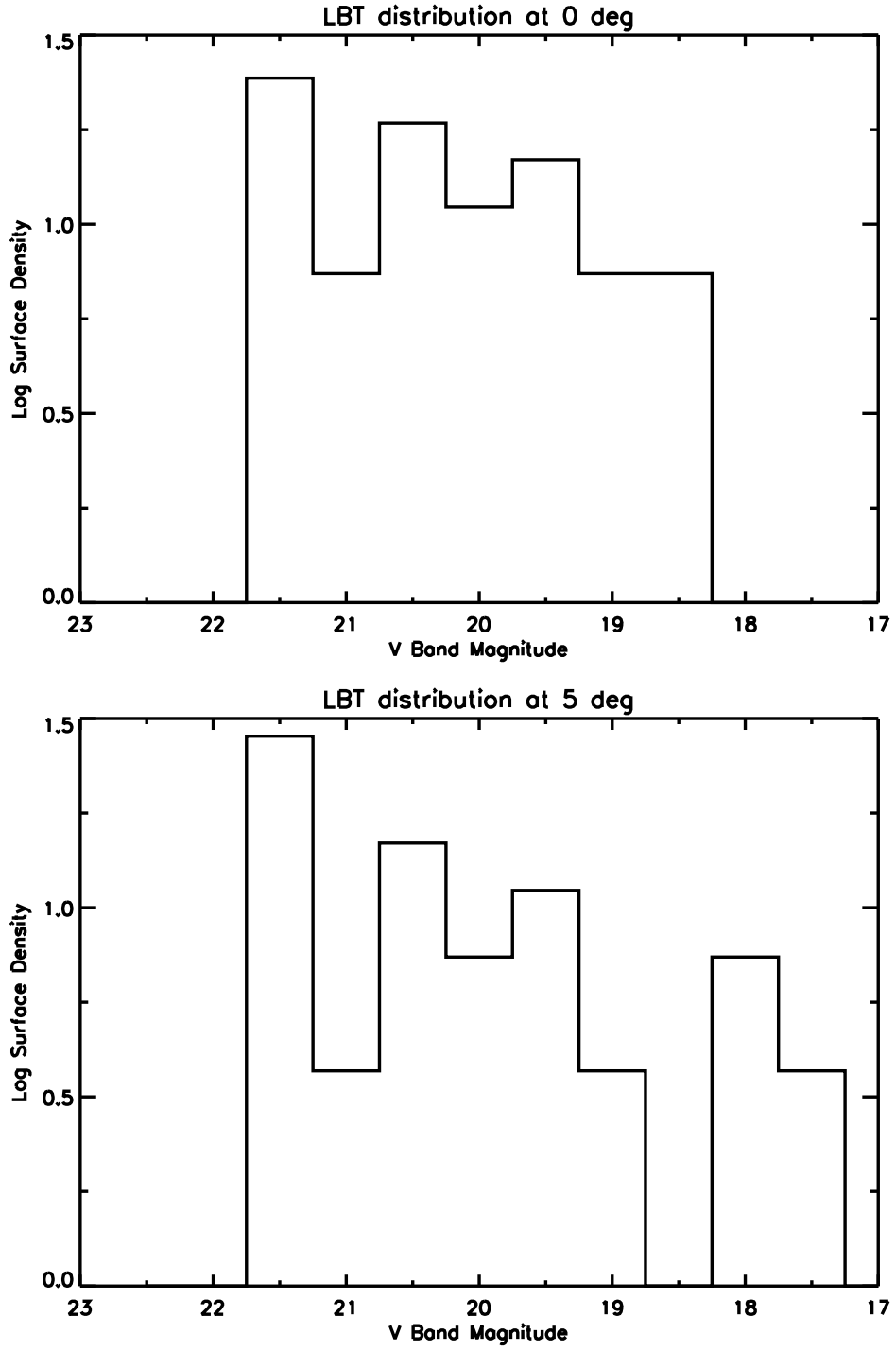


Fig. 1.— Magnitude histogram distribution for LBT asteroids at 0° ecliptic latitude ([a], upper) and 5° ecliptic latitude ([b], lower).

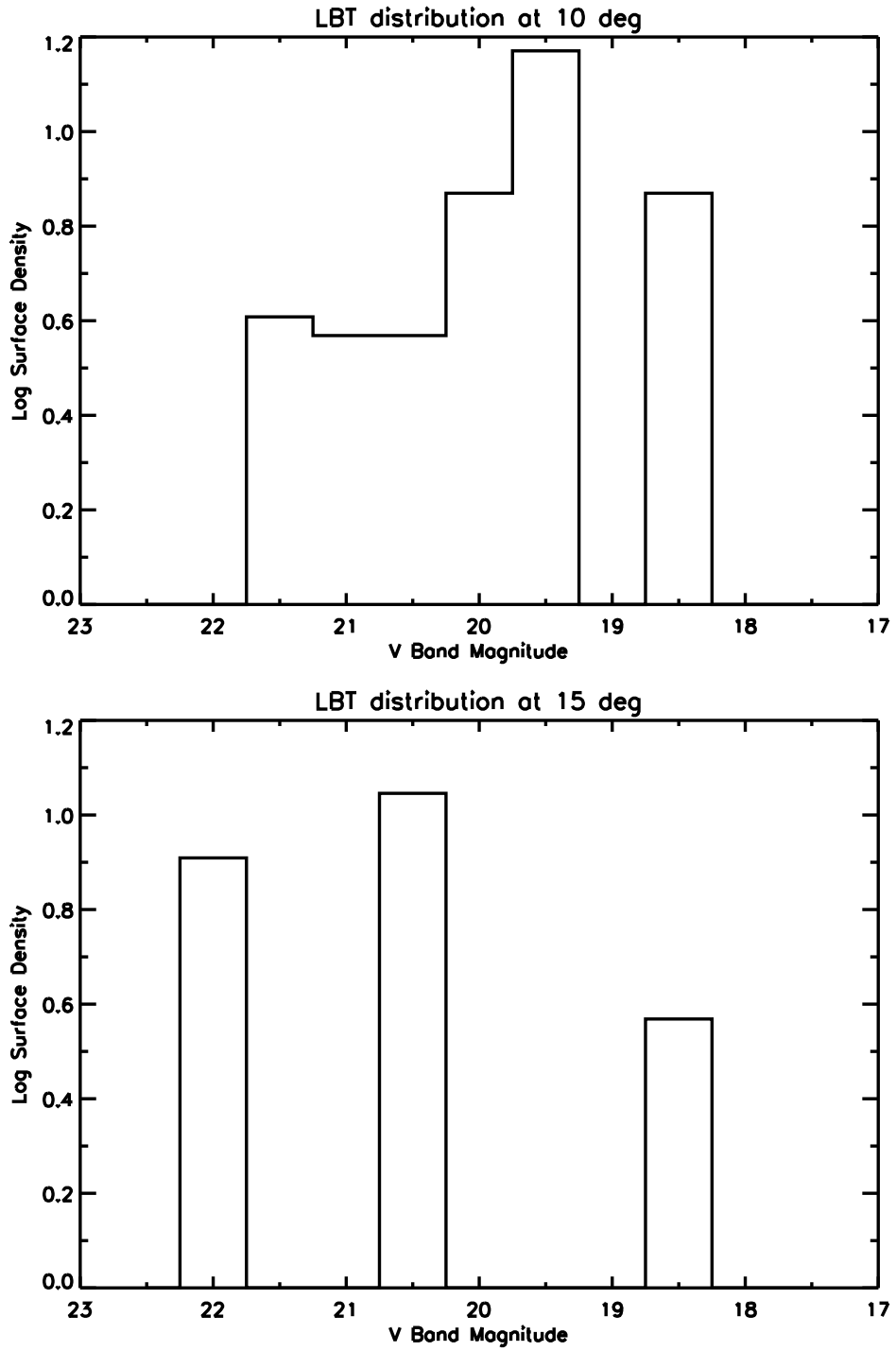


Fig. 1.— *continued*: Magnitude histogram distribution for LBT asteroids at 10° ecliptic latitude ([c], upper) and 15° ecliptic latitude ([d], lower).

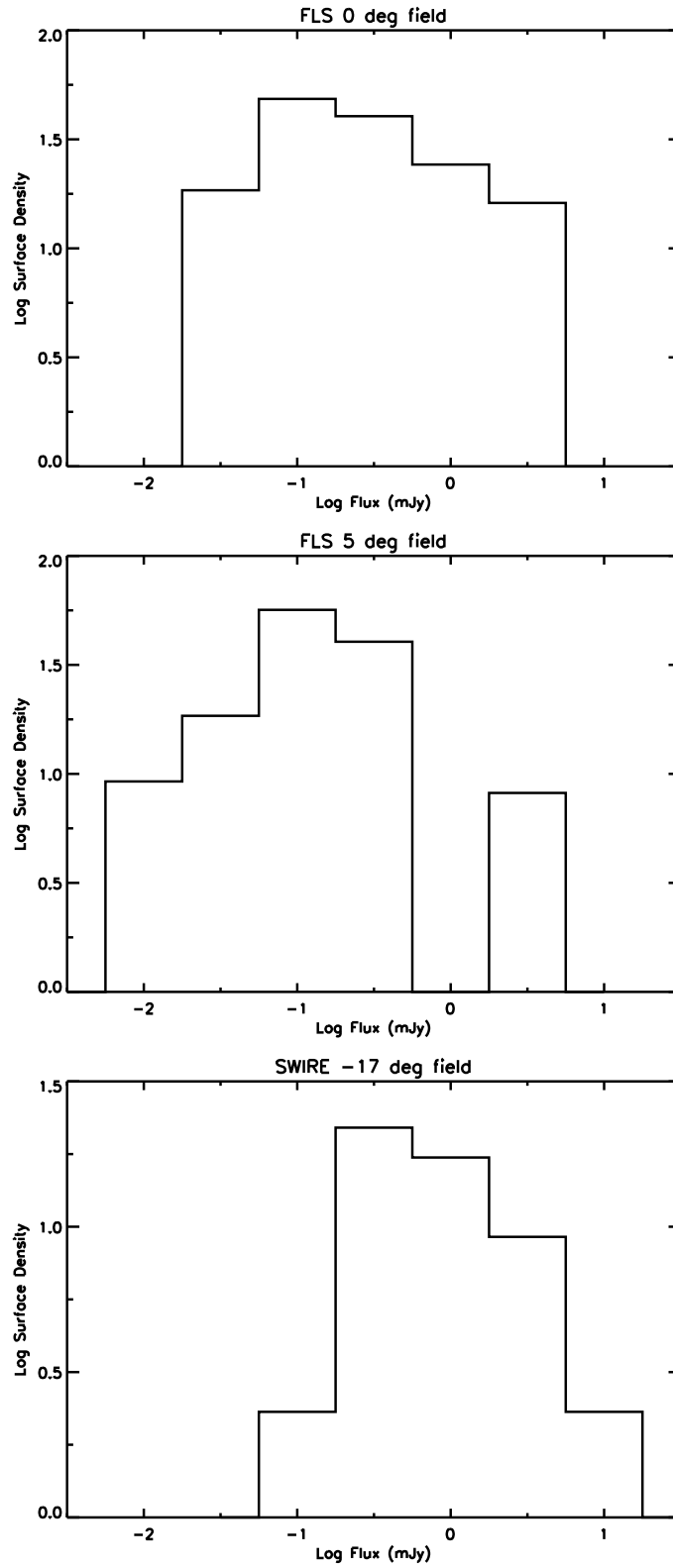


Fig. 2.— Magnitude histogram distribution for *Spitzer* FLS asteroids at 0° ecliptic latitude (upper), at 5° ecliptic latitude (middle), and at 17° ecliptic latitude for the SWIRE field (bottom).

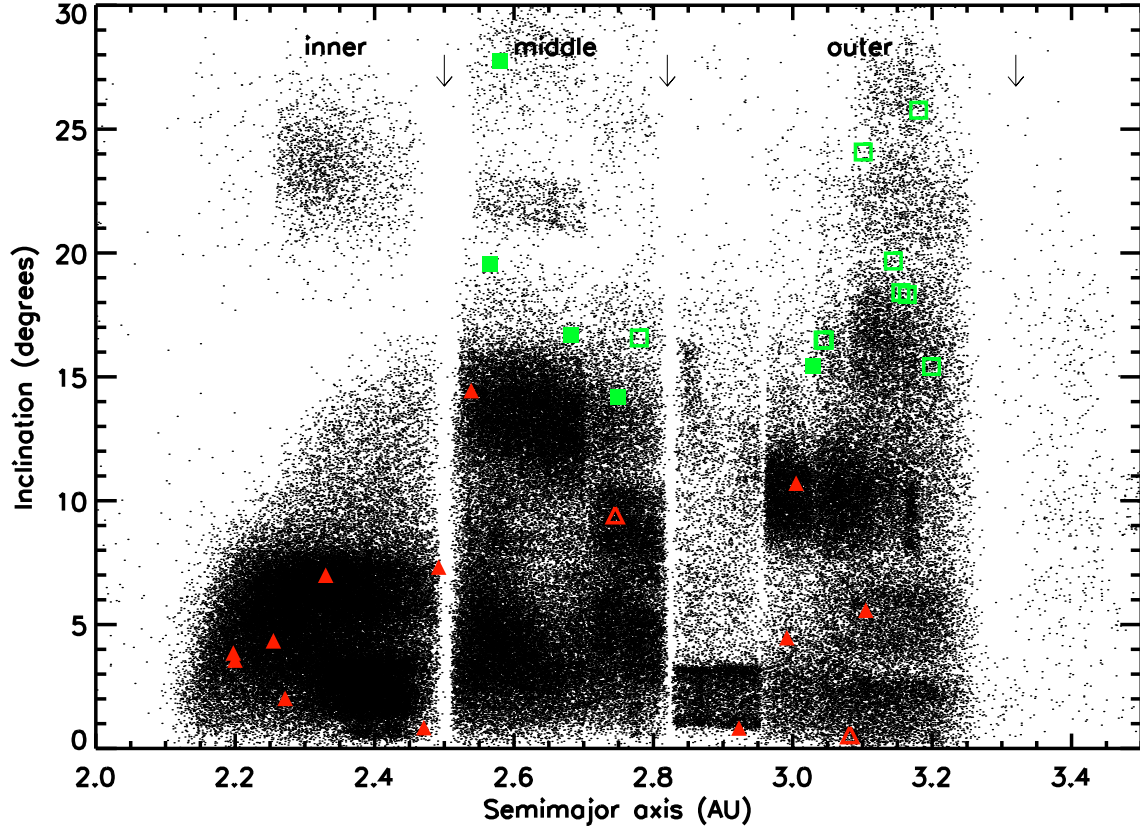


Fig. 3.— Proper orbital elements a (orbital semi-major axis) vs. i (orbital inclination) of asteroids. The *Spitzer* SWIRE and FLS asteroids are denoted respectively by green squares and red triangles, while 207,942 numbered asteroids with orbital elements in the ASTORB files are plotted with black dots. Open colored symbols indicate asteroids with derived albedos, p_V less than or equal to 0.1, while filled symbols denote asteroids with $p_V > 0.1$. The location of the major Kirkwood gaps as defined by Parker et al. (2008) are indicated by the labels and vertical arrows.

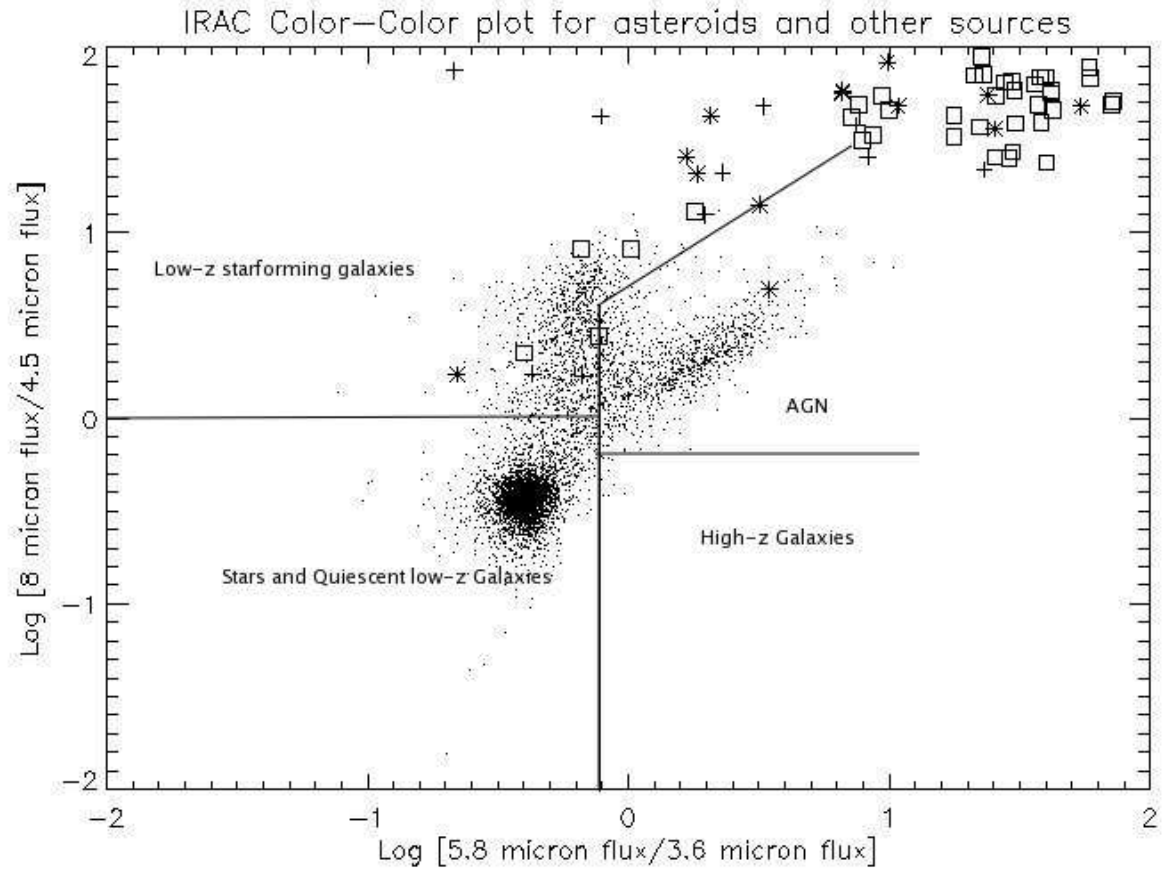


Fig. 4.— IRAC colors of astronomical objects and asteroids. The plus signs correspond to asteroids in the FLS 5° field, asterisks correspond to asteroids in the FLS 0° field and boxes correspond to asteroids in the SWIRE field. This plot is an adaptation of Lacy et al. (2004) as modified by Ryan & Woodward (2006).